IMPACT OF FUEL CELL AND BATTERY SIZE TO OVERALL SYSTEM PERFORMANCE – A DIESEL FUEL-CELL APU CASE STUDY

Boštjan Pregelj[1], Michal Micor[2], Gregor Dolanc[1], Janko Petrovčič[1], Vladimir Jovan[1]

[1] Jožef Stefan Institute, Jamova cesta 39, 1000 Ljubljana, Slovenia
[2] Faculty of Electrical, Electronic, Computer and Control Engineering, Lodz University of Technology, Poland

bostjan.pregelj@ijs.si

Applied Energy, Volume 182, 15 November 2016, Pages 365–375

http://dx.doi.org/10.1016/j.apenergy.2016.08.119
free link: http://authors.elsevier.com/a/1TdOC15eiekkA1

Abstract: In this paper a data-validated power-efficiency model of a diesel-powered fuel-cell-based auxiliary power unit (APU) system is used to investigate the various sizes of the power unit and the battery and to evaluate the optimal choices for specified load profiles. The challenge comes from the FCGEN (Fuel Cell-based power GENeration) EU FP7 project, where such an APU was developed. The system consists of a fuel processor, a PEM stack, and a battery providing power for the startup, shutdown, and for covering load transients; however, the developed prototype system is not optimised. Before redesigning it for mass production, the optimal size of the main components needs to be identified to enable the best possible exploitation of the technology. In this work a case-specific load profile was used and a mesh grid of scenario simulations has been performed using various sizes of the fuel cell with fuel processor as a power unit and the batteries of various capacities as an energy storage unit. For this purpose a scalable APU model, including the BoP component consumption, has been developed. Upon the analysis results, the relation for optimal combinations in terms of efficiency and degradation is proposed and the confronted tradeoffs are discussed.

Keywords: *diesel fuel cell APU; component size optimization; optimal relation; simulation analysis; fuel processor; battery*

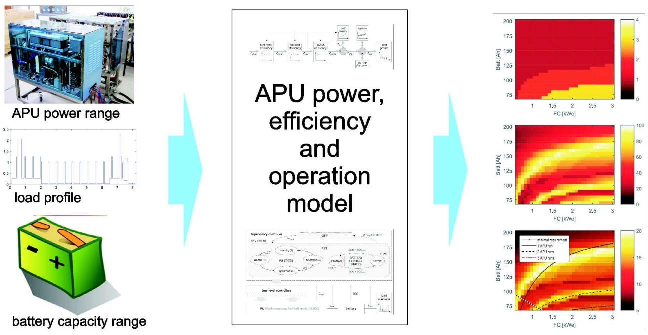

1 INTRODUCTION

Recently, ever more often, new products and applications based on fuel cells with a *Polymer Electrolyte Membrane* (PEM FC) [1], [2] are being launched, and this attractive technology [3], [4] is gathering further momentum. Recently, the FC-based auxiliary power units (APU) have also received increased attention. There is an interest noticed in such products in the vehicle (trucks [5], [6], [7], caravans, busses [8]) and maritime field (yachts [9], [10] and sailboats [11]), as well as in the stationary application market (mCHP, telecom base stations [12], remote, mountain houses, etc. [13]). Such APUs can be fuelled directly by hydrogen as well as by commonly available LPG/CNG or gasoline/diesel fuel [14], [15], [16], [17]. They operate at higher efficiency and with lower noise and pollutant emissions compared to ICE-based units [18]. In the case using one of the ubiquitous fuels, the system has a wide application area but requires the expensive and complex reformer part [19], [20]. Several research projects (e.g., FCGEN [21], DESTA [22], PURE [23], etc.) have been initiated to overcome further obstacles to commercialization and to demonstrate such APUs in real use cases. However, to be successful, several aspects of these systems, namely, economics [24], reliability, and sustainability [25], still require to be further optimised. The cost of initial investment is high, and despite its lower consumption and very low pollutant and noise emissions, the total cost of ownership[1] (TCO) [26] is still too high. Despite recent advances in fuel-cell and reformer technologies and, in part, also in industrialization [27], as well as control [28], [29], [30], [31] and monitoring [32], [33], the current implementations still have some margins

[1] TCO is a financial estimate intended to help buyers and owners determine the direct and indirect costs of a product or system. It is a management accounting concept that can be used in full cost accounting or even ecological economics where it includes social costs.

in efficiency and durability but predominantly exceed cost and size targets, owing mostly to two reasons:

- Prototype or small series production
- Suboptimal components matching

An important design phase, addressing the latter, is the selection of system components, the main parts as well as BoP components. Only by selecting the operating-condition adapted and closely-matched components, power-wise, can all parts of the system be exploited optimally, enabling the system as a whole to approach the theoretically optimal performance and durability level. In recent studies, the issue has been tackled for the fuel cell vehicle [34], [35] and for the solar/wind power generation [36], [37], [38] applications, but with other incentive and approach.

In such a complex system, the experimental trial-and-error approach cannot be efficient. The time- and cost-effective alternative is to perform this in simulation [8], [12]. However, one has to bear in mind the possible offsets of the model from the real environment and the simulation results have to be evaluated properly. Experience and practice point towards more weight on simulation in the early phases and on real-world experimentation in the late development phases.

To a good effect, such approach was used in a simulation case study [39], where a diesel fuel-cell-based APU was used in an anti-idling application [40], [41] to support the selection of the most suitable battery type for the FCGEN project APU. In the anti-idling case, the APU has to feed the needs of the truck, i.e. heater, air-condition, cooker, electronic equipment, etc. Its main objective is to be able to stand a full night of use independently while achieving the highest possible efficiency and requiring the least starts to minimise the degradation effect.

During the late development stages of the FCGEN APU and commissioning, it was observed that better power matching of sub-components is possible. In this sense, to enable the exploration of the exploitable space, the similar approach has been used here to inspect the sizing of the power unit (PU) and the battery and to research the parameters that govern the selection of the most suitable combination.

To perform this study, we originated from previous work [39], which comprises the efficiency and power models of the main PU components, the battery model and the power consumption profile. The model was upgraded from its predecessor to allow power scaling, and it also features data-validated BoP component power consumption characteristics. With this setup we have investigated the operational properties of the power unit (PU) and battery size for a truck on-board diesel-powered FC-based APU system for a variety of APU and battery sizes and generated a heat-map of efficiency and number of starts to facilitate the decision.

The paper first presents the APU, the power-efficiency model, described in more detail in [39], with additional characteristics tuned from a real system operation. Follow the descriptions of the control system and of the APU loads with their profiles for the truck's onboard application. The battery and PU combinations are evaluated in the simulation and the findings are summarised relating to overall efficiency, degradation, price, and other aspects of practical use.

2 SCIENTIFIC APPROACH

The main idea of the presented work is to feed a model with the desired load profile as well as the interesting ranges of the power module and battery. After running the simulations, the residuals are generated automatically and presented in the form of informative heat-map plots. To do that, the model has to describe the interesting process parameters, i.e. power flows and efficiencies, as well as model the autonomous operational behaviour of the APU, i.e. the control system.

2.1 THE APU PROCESS

The APU system, developed within the FCGEN project, is composed of two main parts. The fuel processor (Figure 1, right unit) is used to convert the diesel into hydrogen-rich reformate gas and the fuel cell (Figure 1, within left unit) to transform that into electricity.

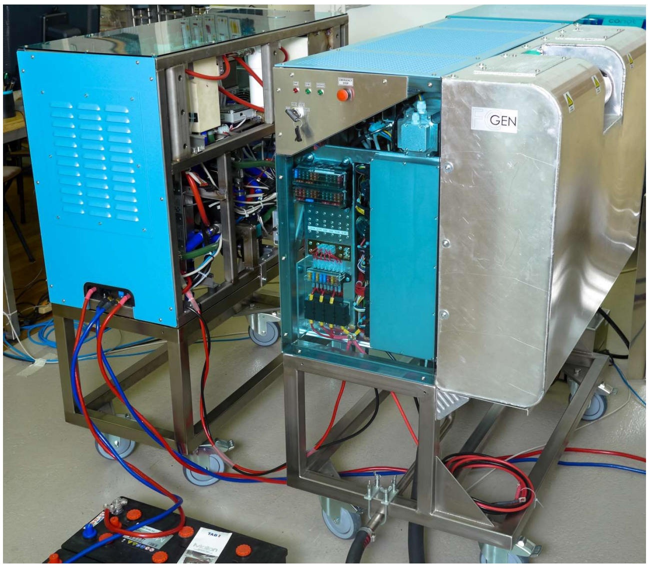

Figure 1. The diesel-powered FC-based APU developed within the FCGEN project during final demonstration. In the figure, the fuel processor

module stands on the right side and the power-generation fuel cell module on the left.

The simplified PU process scheme, showing its main components and process path, is presented in Figure 2. The diesel reforming path comprises autothermal reformer (ATR) [42], [43], [44], desulphurization unit (DS), and water-gas-shift (WGS) and preferential-oxidation (PROX) reactors for carbon monoxide conversion [45]. Thus, prepared reformeate gas enters the fuel cell (FC) anode, where it is converted to electricity with controlled H_2 utilization factor. The anode off-gas containing the residual H_2 is then combusted in the catalytic afterburner (CAB) and the generated heat is used to preheat the steam entering the reformer and to completely burn potential other combustible or harmful compounds. The electrical energy generated by the fuel cell is treated by DC/DC converter, which is controlled to perform safe battery charging and provide power to the loads.

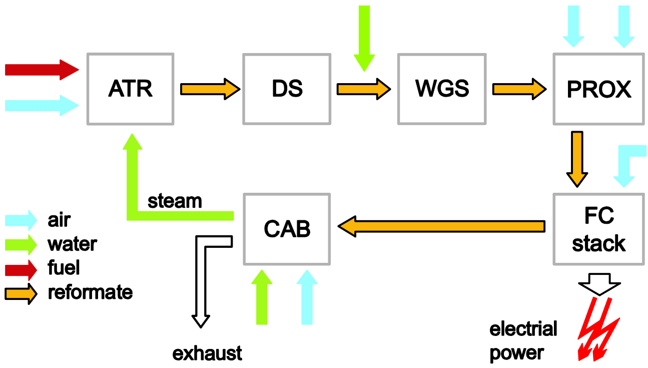

Figure 2. The FCGEN diesel fuel-cell based PU process layout with main reactors and reactant flows, without cooling loops

The developed prototype unit is a complex system consisting of numerous subsystems and components:

- Fuel processor reactors for diesel reforming and S/CO treatment
- Fuel-cell stack
- Power conditioning modules (DCDC converter, power distribution board for efficient BoP power supply)
- BoP components – 38 actuators (pumps, blowers, valves) and over 60 sensors (various temperature sensors, pressure sensors, flow meters, gas sensors)
- Electronic Control Unit for overall control and remote operation/monitoring

The final APU is able to operate autonomously and provide 3 kW of electrical power to the load. Due to relatively slow dynamics of chemical processes imposed predominantly by fuel processor, a battery is a required part of the system that compensates for the difference between PU power and load demand as well as powers the startup and shutdown procedures. The main subsystems are presented in a basic system scheme in the upper part of . .

The APU development process took several iterations in the design phase, but only a single system has been built within the project. Throughout the system commissioning, numerous improvements were made, but still the prototype could not fully achieve all targets; predominantly, the power range and the efficiency were issues. This was mostly due to discrepancies of the BoP components and heat transfer coefficients from their design values, possibly further contributed to by slightly deactivated reactor catalysts after pioneering experiments. All that led to the operational FC stack H_2 utilization factor being reduced to 65% from the designed 70-80% interval and the maximal experimentally achieved thermal load reaching 85%. In the simulation, we have, therefore: *i)* extrapolated the experimental data to 100% operating range, *ii)* used the design value for H_2 utilization, and *iii)* used the manufacturer's data [46] for the reformate-fuelled FC stack efficiency.

2.2 APU SIMULATION MODEL

The simulation model includes all interplaying APU process components, namely the PU, the battery and the load. Within the PU there are the fuel processor and the fuel-cell stack, supported by BoP components and a power converter. From the perspective of the study, the power flows and losses have to be modelled, while other aspects are less important. Where relevant, the process dynamics are compensated for by slow ramps implemented in the control. The control, being the final part defining the fuel flow (consumption) based on load demand, is described in the next section. The scheme of the process model, describing how the fuel energy is converted and how the energy losses are distributed among subsystems, is presented in the lower diagram of . . In the following, the model of a 3 kW net electric (kWe) APU, implemented in the Matlab/Simulink environment [47], and the model-scaling functionality are described in more detail.

2.2.1 FUEL PROCESSOR, FUEL-CELL STACK AND DC/DC CONVERTER MODELS

The model of the system used for this study is composed of the lumped power-efficiency models of the fuel processor (FP) [42], [43], fuel-cell stack (FC) [46], power DC/DC converter and battery. For the fuel processor and the stack, the manufacturers' load-dependent characteristics, recalculated to stack current, were used, presented in the left and middle chart of Figure 4. For the stack efficiency, the H_2-utilization-affected values are used. The 70% and 80% H_2 utilization factors are used at 50% and 100% fuel processor thermal load, respectively, with linear interpolation in-between. The lower (e.g. 70%) H_2 utilization factor translates to more heat energy generated in the CAB by burning the residual H_2, which is required to maintain sufficient steam quality (temperature) in the ATR at lower (50%) fuel processor load. This is important, as for the ATR, constantly operating above 900°C, heat losses remain at the same level regardless of the operating point. Hence, they are relatively much higher at the lower end and need to be compensated. For the DC/DC converter efficiency, a value of 95% was obtained by system measurements. The model background is comprehensively described in [39].

2.2.2 POWER CONSUMPTION OF BOP COMPONENTS, STARTUP AND SHUTDOWN

The successful PU operation is reliant on 38 actuators (9 valves, 13 pumps, 16 compressors/blowers). Part of them operate constantly regardless of the APU operating point (valves, cooling water pumps), whereas others follow the operating point. The BoP components power consumption has been measured during experiments. The measured values for the fuel processor load range of 50-85% are given in Table 1. Within the model, approximation (1) is used to enable simulation up to 100% load. A second order polynomial is used due to the inherent quadratic power/flow dependence of the blowers, the main BoP power consumers.

$$P_{BoP} = 0.0234 \cdot I_{stack}^2 + 3.4497 \cdot I_{stack} + 171.9586 \quad (1)$$

The measurements and the approximation (1) are presented in the right chart of Figure 4.

Table 1. Measured BoP consumption at different operating points for 3 kWe APU system.

Stack current (A)	BoP power (W)
52.1	420
57.1	450
65.0	490
71.4	530
78.0	580
84.5	640
91.0	680

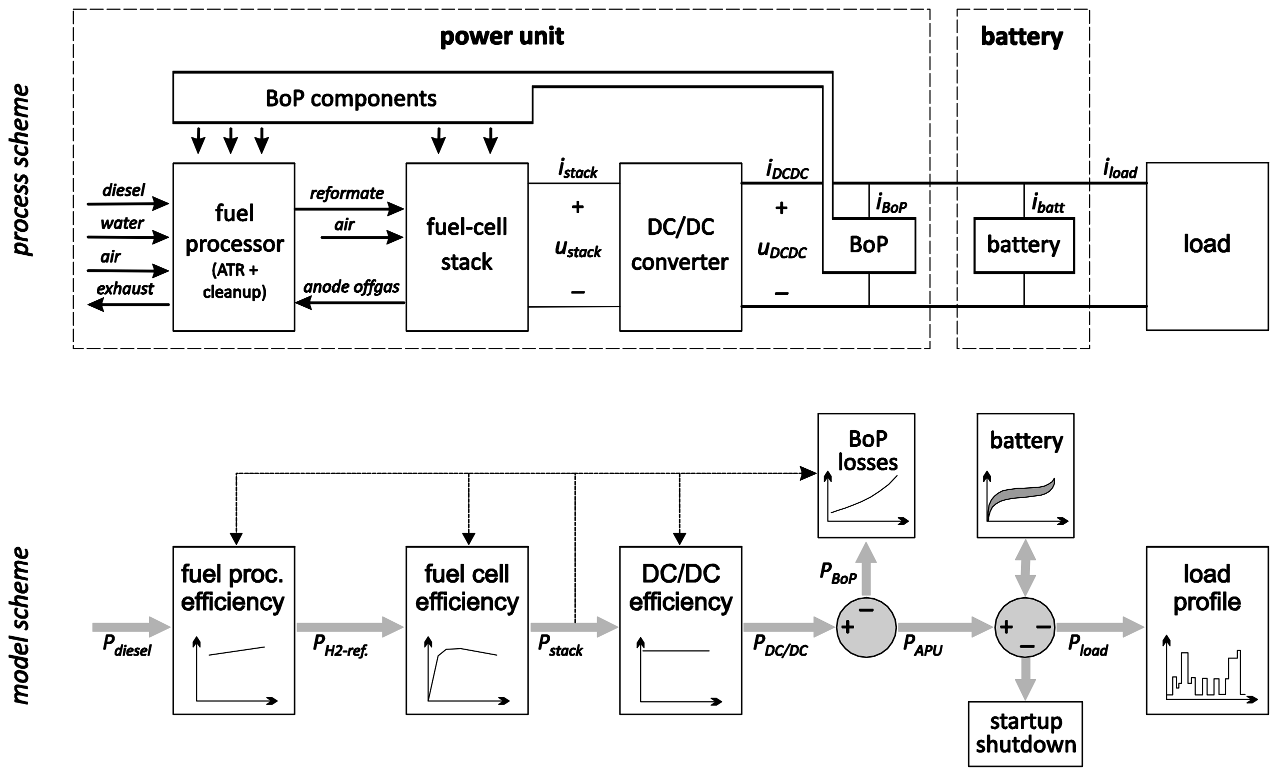

Figure 3. Study-relevant concept schemes of the APU system with main PU and battery sub-systems (above) and the APU power-efficiency model (below). The bold grey line represents the energy flow and the dotted black line describes the fuel-cell stack power, i.e. current, which is input to model characteristics

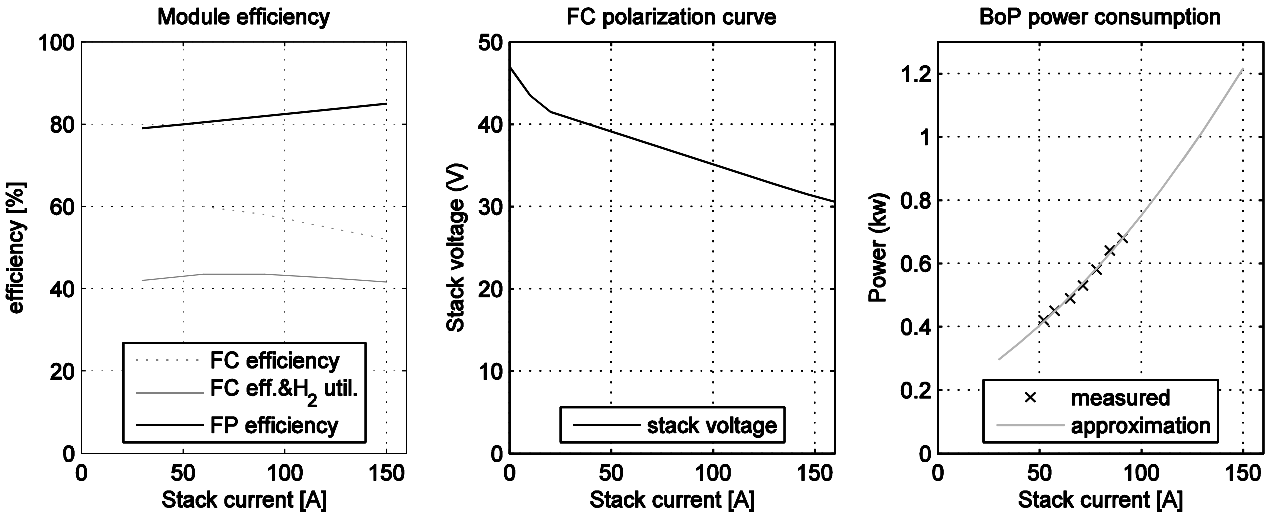

Figure 4. Load dependent characteristics for 3 kWe PU: FP and FC efficiencies (left), FC polarization curve (middle) and BoP power consumption (right).

Besides the operation regime, there are two important phases where BoP components consume notable amounts of power, namely, the startup and the shutdown, as the reactors are preheated to the required temperatures before the operation and cooled down afterwards. The preheating energy is provided by the catalytic startup burner (SB), burning diesel with an average power of 3 kW. Additionally, the blowers are required to take the heat from the SB exhaust and spread it through the fuel-processor reactors. The main electrical power consumers are blowers for the SB (500 W) and for the fuel processor (450 W). The 1 kW average power and duration of 0.5 hours have been used. On the other hand the shutdown procedure takes 0.25 h with an average consumption of 0.3 kW.

2.2.3 THE BATTERY MODEL

The macroscopic nature of this study minimises the benefits gained by detailed battery operation analysis. Therefore, fast, practical and understandable models were in favour. For comparability with the previous work in [39] and [28], the model from the Matlab/Simulink in the SimPowerSystems library [47] was used for modelling the battery. The 26 V Lithium-ion battery [49] considered in the FCGEN project [39] has been chosen since it allows a wide range of charging currents without any effect on its longevity [50], [51] and brings benefits in terms of size and weight, which are the important factors on-board any vehicle.

2.2.4 SCALABILITY

The PU model has been developed in a way that it allows for nominal power level scaling. The fuel-cell voltage model is scaled by variable membrane size, the efficiency characteristics of the fuel cell and fuel processor are scaled based on scaled nominal stack current, and the BoP component power consumption is scaled in both axes. The Matlab's battery model allows simple scaling in terms of voltage or capacity, and the latter was used.

2.2.5 LOAD PROFILES

In order to be able to simulate the model and generate relevant data, the further load parameters were also defined: daily load profile and power consumption of the BoP components during operation (load-dependent characteristics). The truck-anti-idling case loads and their profile used in this study have been identified in [39], as shown in Figure 5. The total night-stop energy consumption of the truck loads sums up to 2.89 kWh for the summer and to 3.95 kWh for the winter scenario. Presuming a single PU operation per night, another 0.575 kWh consumed by startup/shutdown has to be added to that number.

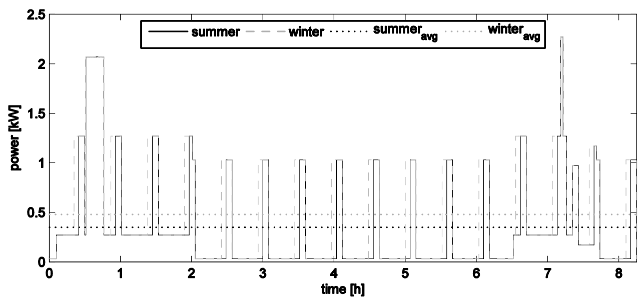

Figure 5. Truck loads power profiles for the summer and winter scenarios and their average values.

2.2.6 APU OPERATION AND CONTROL MODEL

The objective of the control system is to ensure the APU system is able to provide power at any time and at the same time to optimise the system efficiency and preserve the battery. To do this effectively the control system has a hierarchic structure, shown in Figure 6. There, on the higher level, the battery state of charge is monitored and the control automaton operates the APU to charge the battery cyclically. On the lower level the control loops are assumed to maintain operating conditions at the design point.

In general the APU system operates in the following way: In the *standby* state the *FP/FC* is stopped and the battery is used to provide power to the load. When the battery state of charge (SOC) meets the lower limit, the transition to *startup* state is made. After the startup procedure is completed, the *operation* state becomes active. In this state the power is first ramped up to 100% and then controlled to power the loads [52], [53] while ensuring safe battery charging. This way, the APU is mainly operated at nominal power (100%), yielding the highest efficiency and only reduced to prevent exceedingly high battery charging in case the load consumption decreases [28]. All the FP/FC power level transitions are executed via a ramp that compensates the process dynamic adequately and ensures healthy operation of the fuel processor (good diesel conversion) as well as the FC stack (no reactant starvation). When the battery SOC hits the upper limit, the transition to *shutdown* state is made, and the system (FC stack, reactors and piping) is purged appropriately and all components are cooled down. After that the control switches back to *standby* state.

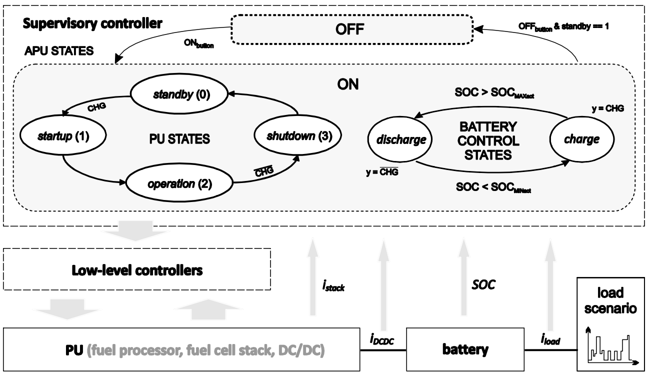

Figure 6. The hierarchic structure of the APU control: the upper (APU) and the supporting (FP/FC and Battery) control automata

The main challenge of the control system is to strike a balance between the safety, robustness and optimality of operation. The PU startup procedure has to be initiated at a point where the battery has enough power to power the loads and PU startup before going below lowest allowed SOC value. A similar but less critical issue is repeated at the upper SOC limit, as the battery must not be overcharged during the power-down transition. The effective upper and lower SOC limits are calculated each control iteration (time step) in a way that also considers the recent load average, as described [39]. The equations governing the threshold values are:

$$SOC_{MINact} = SOC_{MIN} + \left(\frac{P_{start}}{U_{batt_0}} + I_{loadAVG}\right) \cdot \frac{t_{start}}{C_{batt}} \cdot 100\% , \qquad (2)$$

and

$$SOC_{MAXact} = SOC_{MAX} - \left(\frac{P_{act}+P_{min}}{2\, U_{batt0}} - I_{loadAVG}\right) \cdot \frac{t_{decr}}{C_{batt}} \cdot 100\%, \qquad (3)$$

where SOC_{MIN} and SOC_{MAX} are the nominal SOC limits, P_{start} is the startup consumption of the BoP components, P_{act} and P_{min} are the actual and minimum PU power values, t_{start} and $t_{decr}$are the startup and power ramp-down times, U_{batt_0} is the nominal battery voltage, C_{batt} is the battery capacity in Ah, and $I_{loadAVG}$ is the filtered value of the load current, representing the short-term average, which is defined by

$$I_{loadAVG} = I'_{loadAVG} \cdot (1-\beta) + I_{load} \cdot \beta, \qquad (4)$$

where $I_{loadAVG}'$ is the value from the previous sample and β is the forgetting factor with the value of 5×10^{-5} with a sampling time of $1s^{-1}$. The $I_{loadAVG}$ is used for SOC thresholds and for power set-point calculations to prevent fast variations of the calculated values when loads switch on/off instantly.

So far, only the component models have been described, although the APU operation is also subject to limitations on power parameters and their transition rates:

- the minimal and the maximal power levels imposed by FP/FC system
- the power transition rate imposed by FP dynamics
- the maximal charging current imposed by battery.

These constraints are also implemented in the control algorithm, which defines the stack current set point in the *operation* state. It is subject to two limitations, the maximal APU output and the maximal battery charging current, defined by

$$i_{stack_{ref}} = \min\left(i_{stack_{max_{APU}}}, i_{stack_{max_{BATT}}}\right), \qquad (5)$$

The stack current is limited by the smaller of the APU and battery limitations:

$$i_{stack_{max_{APU}}} = \frac{i_{max_{APU}} \cdot U_{batt_0}}{U_{stack_{maxPow}}} \;, \quad i_{stack_{max_{BATT}}} = \frac{\left(i_{max_{BATT}} + i_{loadAVG}\right) \cdot U_{batt_0}}{U_{stack_{maxPow}}} \;, \qquad (6)$$

where U_{batt_0} is the nominal battery voltage, $i_{max_{BATT}}$ is maximal battery charging current, and $U_{stack_{maxPow}}$ is the stack voltage at maximal power. A typical APU operation cycle is shown in Figure 7 with the following essential points denoted:

1. Battery SOC below SOC_{ACTmin} detected, ***startup*** *state activated*
2. Startup procedure finished, ***operation*** *state activated*
3. Battery SOC above SOC_{ACTmax} detected, *power ramp-down initiated*
4. APU power down to 50%, ***shutdown*** *state activated*
5. Shutdown completed, ***stand-by*** *state activated*

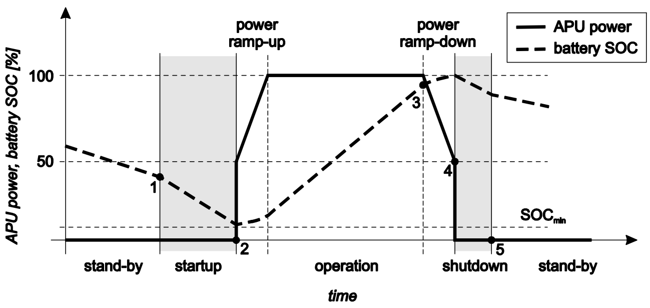

Figure 7. Typical APU operation cycle with denoted mode-switching points

3 SIMULATIONS

The simulations consider the daily load scenarios presented in Figure 5, described in detail in [39]. Furthermore, the following presumptions are taken:

a) the truck stops in the evening with the battery fully charged (SOC 100%), from which all the night-stop electric loads are supplied;
b) at the end of the night stay, when the main engine is started, the APU must be in *standby* mode, or *shutdown* procedure initiated if in *operation* mode;
c) the battery is refilled to 100% during driving by the truck alternator, as within the project scope the APU cannot be operated during driving.

In Figures 8 and 9, the examples of two scenarios, each with a different PU-battery combination, are presented, both ending with a highly charged battery. In Figure 8 an example of winter scenario simulation for the combination of 160 Ah battery and 2.025 kW APU is shown. For this, the actual scenario is as follows. The truck with a fully charged battery stops in the evening for the duration of 8.25 h.

During this time the APU system is subjected to the load profile (black line in upper chart). Initially, the battery powers the truck loads; at time 5.55 h, the active lower battery SOC limit (2) is reached, and the startup procedure is initiated. At time 6.15 h, the power generation starts and the excess power charges the battery. The end-of-stay (8.25 h) is reached just before the upper battery SOC limit (3) is reached; therefore, the shut-down is powered by the truck alternator.

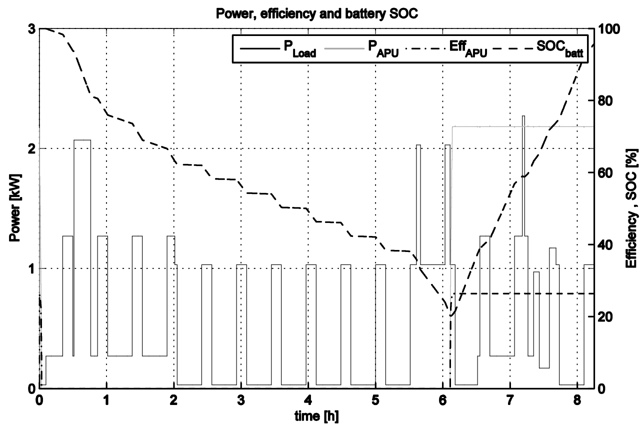

Figure 8. Time plots of winter night-stop simulation with 2.025 kWe[2] PU and 160 Ah battery; the chart presents the PU power (grey) and truck load (black) on the left-hand scale, and the APU efficiency (dash-dotted) and battery SOC (dashed) on the right-hand scale.

In Figure 9 the plots for the summer scenario simulation with 75 Ah battery and 1.425 kW APU are shown, where the PU needs to be started twice. Each time before the battery charge phase, a larger load consumption can be observed, owing to the APU startup procedure consumption.

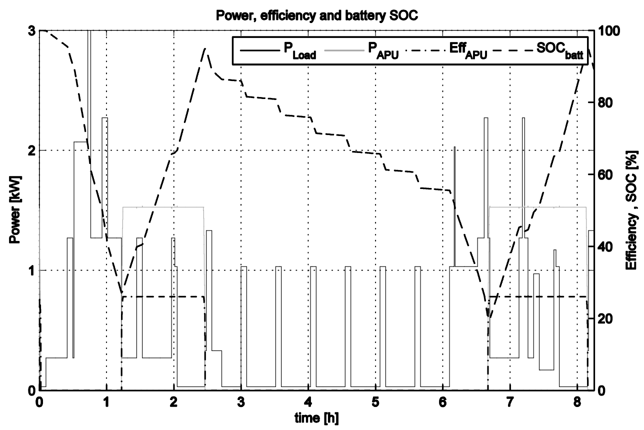

Figure 9. Time plots of summer night-stop simulation with 1.425 kWe PU and 75 Ah battery configuration, requiring two starts; signals as in Figure 8.

[2] For the APU the net electric output power is used (kWe), and the fuel cell power is greater to cover the BoP consumption

3.1 MULTI-SIMULATION STUDY

In order to analyse the system and to research a rule to pick the most suitable parameters, a grid with the varying battery capacity and PU output power sizes was researched and analysed. On the first attempt only a sparse 4 × 4 grid was investigated, yielding preliminary results [48] that proved inconclusive as they did not demonstrate any phenomena. To provide a better insight, a dense experiment grid was evaluated in this work, with 1782 combinations considered:

- 33 APU evenly spaced net electric nominal power levels (0.6 kW – 3.0 kW)
- 27 evenly spaced battery sizes [70 Ah (~1.3 kWh) – 200 Ah (~5.2 kWh)]
- 2 scenarios: summer and winter (consumption for heating is higher than cooling)

It is worth noting that the batteries with a capacity lower than 70 Ah were not investigated due to high and increasing load profile at the beginning of either scenario, which prevented the used control algorithm from initiating the APU startup soon enough. As a result the battery got completely drained out, stopping the simulation early.

4 EVALUATION AND RESULTS

For this study we focused on two operational parameters. The first is the commercially interesting net efficiency and the second is the number of APU starts, importantly influencing system lifetime as well as efficiency. To obtain efficiency, over the simulation time, for each experiment all the power flows and the operational efficiency were logged. Based on those, the startup and shutdown energy, the number of APU starts during the night stay and the net efficiency were calculated.

4.1 EVALUATION PRESUMPTIONS

Additional presumptions have been made to enable a fair comparison of the experiments:

a) at the end of the simulation, each battery is charged with appropriate current to 100% using truck alternators;
b) in case the APU is in *operation* mode at the end of the simulation, the whole shutdown energy is provided by the main ICE alternator;
c) in case the APU is in *shutdown* mode, the energy for the remainder of the shutdown is calculated based on the remaining time of the procedure;
d) the efficiency by which the electricity is produced by the main engine-powered truck alternator is considered at 10%.

4.2 EVALUATION CRITERIA

For evaluating the efficiency, operational efficiency could be used; however, by doing this not all the losses implied are taken into account. A better option is to measure the useful energy, the one consumed by truck loads, against the complete energy, required to provide the useful energy.

The energy, consumed by loads, i.e. useful energy, is obtained by integrating the load power:

$$E_{load} = \int_0^{8.25} P_{load}\,dt, \tag{7}$$

The total fuel energy consumed for powering a single night stay is then obtained by:

$$E_{fuel} = \int_0^{8.25} P_{fuelAPU}\,dt + E_{fuelSB} + \frac{\int_{t_{night\ end}}^{t_{batt\ full}} P_{batt\_fill}\,dt + E_{stop}}{\mu_{ICEel}}, \tag{8}$$

where:

- $P_{fuelAPU}$ is the power of flow of the diesel consumed by the APU
- E_{fuelSB} is the energy of the diesel, consumed by startup burner
- P_{batt_fill} is the battery charging power from the truck alternator
- $t_{night\ end}$ is the time at the end of night stop
- $t_{batt\ full}$ is the time when battery is filled back to 100%
- E_{stop} is the energy consumed during APU shutdown phase in case it is still active after night stop ends (8.25 h)
- μ_{ICEel} is the efficiency of the diesel truck alternator-produced electricity (considered 10%)

The total efficiency of the night-stop electricity production is then defined as the ratio of the energy required by truck loads E_{load} and the total fuel energy (8) consumed by both the APU and the truck engine to produce the electricity for the night stop as

$$\mu_{tot} = \frac{E_{load}}{E_{fuel}}, \tag{9}$$

Based on this, the efficiency values have been calculated for all simulations. The number of generated values is large, and for illustrative representation the heat-map plots were generated, as presented in Figure 10. Since all system components are scaled accordingly and the APU is considered to run at optimal operating point at all times, the differences in APU operational efficiencies are minimal, averaging around 26+-0.5%, as can be seen in the top charts of Figure 10. The values are rather low; however, they are based on the in-project-developed prototype system, which took many compromises, while a fully optimised system should reach around 35%.

In Figure 10 two phenomena are worth noting. First, in the end-of-simulation SOC chart for summer scenario, there is a very low-value line for 165Ah battery. This results from the APU startup being initiated (startup energy consumed) and night-stay finishing before the APU actually started filling the battery. Second, in several charts, some irregularities appear at lower battery capacities due to insufficient resolution (i.e. too large battery size step), as the texture becomes denser there.

4.3 FINDINGS AND IMPLICATIONS

After performing the evaluation of simulation data, summarised in Figure 10, several observations can be made regarding component sizing. Moreover, a relation between the battery and the PU size, while taking into account the average load, night-stay duration and number of starts that can be formulated. For initial impression a the parameters and the performance comparison of the best single-starting, the best double-starting FC APU and a battery-only setup is made in Table 2.

Table 2. Performance comparison of FC and battery-only APU setups.

Scenario (total load)	Summer (2.89 kWh)	Winter (3.95 kWh)
Battery only, alternator fill-up	***165 Ah battery***	***225 Ah battery***
Fuel consumption	32.0 kWh (3.15 l)	43.7 kWh[3] (4.3 l)
Efficiency	9.0%	9.0%
Single-starting FC APU conf.	***1.275 kWe PU, 120 Ah battery***	***2.025 kWe PU, 160 Ah battery***
Fuel consumption	17.3 kWh (1.70 l)	22.0 kWh (2.16 l)
Efficiency	16.7%	17.9%
Double-starting FC APU conf.	***1.275 kWe PU, 70 Ah battery***	***1.275 kWe PU, 80 Ah battery***
Fuel consumption	21.7 kWh (2.13 l)	25.7 kWh (2.53 l)
Efficiency	13.4%	15.4%

[3] For winter scenario a battery of this size has not been investigated in the study and a linear approximation is used to obtain the value.

4.3.1 MINIMAL REQUIREMENTS

The minimal component sizes are governed by the peak and average load, as well as the APU startup energy. Concerning the average load, the battery has to at minimum provide energy for the APU startup and for the truck loads during startup. Complementarily, the PU has to be able to charge the battery and power the loads while charging. In the optimal case, discussed in the next section, the time required to fully charge the battery is equal to the time remaining till the end of the night stay after the discharge. On the other hand, concerning the peak load, both the battery and the power unit together have to at least be able to provide sufficient power, for a certain amount of time

$$P_{APUmax} = P_{PU} + k \cdot C_b \cdot U_{batt} \quad (10),$$

where k is a battery (technology)-specific factor defining maximally rated discharge and C_{batt} is the current equivalent to the capacity of the battery divided by one hour. For example, a standard 100 Ah Lithium battery can safely provide about 100 A, i.e. 2.6 kW (for a 26 V battery). Similar discharge values hold also for NiMH battery. For real use the battery capacity should always be ca. 10-20% higher to compensate for unpredictable cases. Moreover, in this work the use of Lithium battery is considered, whereas in many cases a heavier and larger NiMH battery would be suitable for its low cost and high discharge current capability for load-bumps and APU startups.

At the upper end size, the 165 Ah battery is able to power the summer loads for the whole night without recharging and already makes the PU redundant. A battery of similar size, 170 Ah, is also sufficient to cover all high-efficiency combinations for the winter scenario, making this the largest discussible choice.

4.3.2 HIGH-EFFICIENCY COMBINATIONS

The highest total efficiency value for summer scenario was 16.7%, achieved using PU with a nominal power of 1.275 kWe and 120 Ah batteries, whereas the PU operational efficiency was at 25.8%. However, there is a curved band of high-efficiency combinations, averaging around 16.0%. For the winter scenario the highest total efficiency was 17.9%, achieved using 2.025 kWe PU and 160 Ah battery, with PU operational efficiency at 26.3%. Again there is a whole band of high efficiencies averaging at 17.5 %. To be more precise,

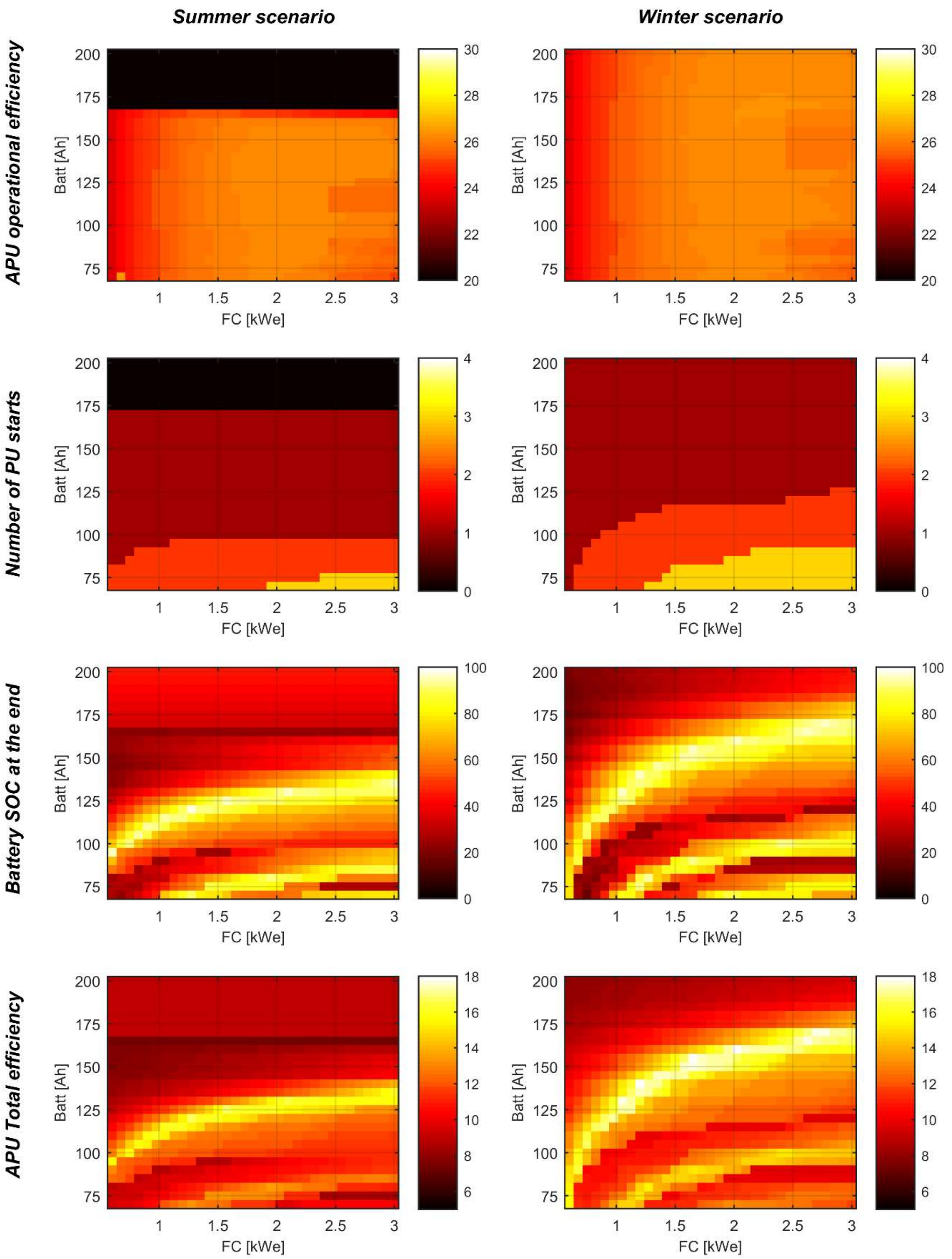

in the total efficiency charts, for either scenario, additional bands with high values appear below the main one. The bands positioned lower on the plot are of lower efficiency due to additional starts of AP related to smaller capacity batteries. These combinations are also less preferred as the excessive number of AP starts affects the long-term component degradation.

Figure 10. Heat-maps summarising the analysis results, covering 0.6-3.0 kW PU range and 70-200 Ah battery capacity range for summer (left charts) and winter (right charts) load scenario. The charts represent the APU operational efficiency (top charts), the number of PU starts (2nd line), the battery's SOC at the end of the simulation (3rd line) and total APU efficiency (bottom charts).

4.3.3 BATTERY-PU RELATION YIELDING OPTIMAL EFFICIENCY

The high values in the total efficiency charts are coinciding with the APU/battery combinations, where the simulations end with a highly charged battery. This is due to almost double APU efficiency compared to the ICE and alternator (see Table 2), which is employed to recharge the battery after the end of stay. Therefore, in optimal case, an integer number of complete discharge-charge cycles should be performed during the night stay. Considering a single APU start per night, given the average truck load, the APU startup energy, and the night-stay duration, the optimal battery capacity is defined by

$$E_{batt} = P_{loadAVG} \cdot (t_{nigh} - t_{chg}) + E_{start}, \quad (11)$$

where t_{chg} is the time that the APU operating at its nominal power requires to charge back the battery:

$$t_{chg} = \frac{E_{batt}}{P_{APUnom} - P_{loadAVG}}. \quad (12),$$

By introducing (12) to (11) and considering the available 80% battery capacity SOC (100%-20%), we obtain a complete formula for optimal battery capacity

$$E_{batt} = \frac{P_{loadAVG} \cdot t_{night} + E_{start}}{0.8}\left(1 - \frac{P_{loadAVG}}{P_{APU}}\right). \quad (13),$$

In the case of multiple APU starts ($N_{start} > 1$), the equation (13) changes to:

$$E_{batt} = \frac{P_{loadAVG} \cdot t_{night} + N_{start} \cdot E_{start} + (N_{start} - 1) \cdot E_{stop}}{0.8}\left(1 - \frac{P_{loadAVG}}{P_{APU}}\right) \quad (14),$$

The overlying plots for both scenarios and one, two or three APU-starts can be seen in Figure 11. Considering the uneven load/time distribution, the approximation fits relatively well. While the single APU start approximation is not best-fitting due to *i)* larger than average load consumption in the last part of the simulation and *ii)* more energy required to charge back the battery (ca. 90% energy efficiency), the two and three AP-start cases fit very well. To obtain a more precise estimation, taking into account further case parameters, a comprehensive analysis beyond the scope of this work is required.

As the high-efficiency band stretches down to the lowest examined values, and when considering the price of both battery and PU is reducing with size, the optimal combination is the smallest, still able to power the peak load. In the presented case, the peak value of truck load is ca. 2.3 kW and the related minimal battery-PU combinations (10) are below values, shown in the charts. Therefore, for an example of 3 kW peak load, the minimal battery-PU combinations are plotted in Figure 11. However, when the PU is in standby, the highest battery discharge current limits the peak load due to non-instant PU startup ($P_{max} = k*C_{batt}*U_{batt}$). This fact has to be considered when designing and operating the APU.

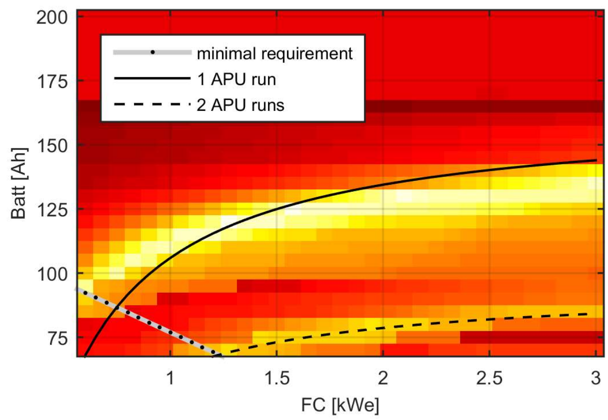

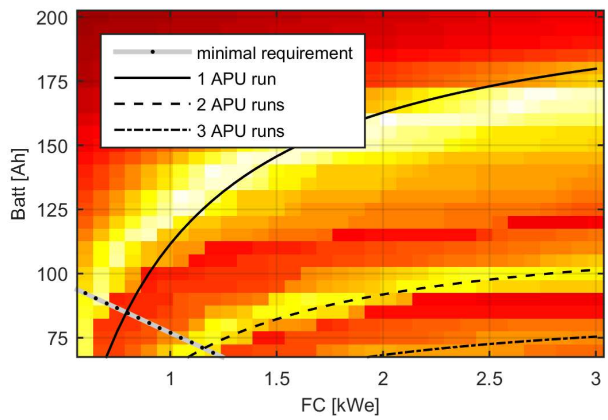

Figure 11. Total efficiency heat maps for summer (upper chart) and winter (lower chart) scenarios, with overlying battery-PU dependency (14) for single (ful line), double (dashed line) and triple-starting (dash-dot line) APU, and with example of minimal battery-PU combinations (black-dotted gray line) for 3 kW peak-load.

4.3.4 OPTIMAL COMBINATIONS FOR BOTH SCENARIOS

In theory, the combination yielding the best results for both winter and summer can be determined. It lies on the cross-section of high-efficiency bands of each scenario. It may be obtained by searching the maximum of the superposed (averaged) total efficiency values for both scenarios shown in Figure 12. Again, the minimums are defined by the peak load.

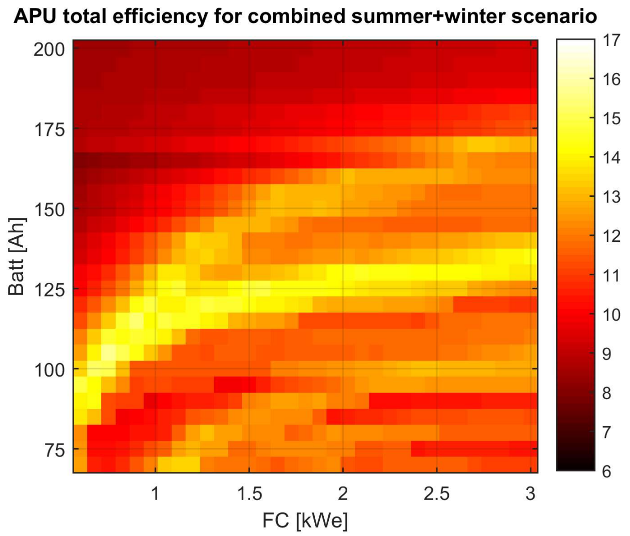

Figure 12. APU total efficiency heat map of the combined equally weighted summer and winter scenarios.

At this point, it is also worth noting that even with combinations outside the high-efficiency bands, this can still be achieved by the use of an intelligent supervisory controller. By learning the approximate load profile or obtaining the future load information elsewhere, the short-term future consumption can be well estimated. Based on it the APU operation can be appropriately adapted by starting the charging or discharging sooner or by temporarily decreasing the APU power, thus reaching the highest SOC value at the end of stay.

5 CONCLUSION

In the paper a systematic simulation approach is used to investigate the optimal sizing of the truck-on-board anti-idling APU system's main components, namely the PU power and the battery capacity. A dense network of possible combinations was investigated using two distinct use case scenarios.

The performed analysis provided a comprehensive insight that could in some points be roughly anticipated before, but by far not to the degree explicitly denoted as achieved after running the simulations. This way, the expected behaviour when changing both APU and battery size can be estimated with decent certainty. Moreover, based on the obtained insight, the relation describing optimal battery size as a function of PU power, average load, duration and desired number of PU starts is formulated, significantly facilitating the APU design process in practice.

Finding the optimal size of the discussed components is essential, as they drive the price and, consequently, the market appeal of the APU system. Furthermore, they also importantly affect the system's efficiency and lifetime. For a more profound insight into system operation and its optimization possibilities, further operational parameters, such as total operating hours, average operating load, model error, etc., could be investigated in future work.

6 ACKNOWLEDGEMENT

The research leading to these results has received funding from the European Union's Seventh Framework Program (FP7/2007-2013) for the Fuel Cells and Hydrogen Joint Technology Initiative under grant agreement n° [277844] and from the Slovenian Research Agency through the Research Programme P2-0001.

7 REFERENCES

[1] Barbir, F. (2005). PEM Fuel Cells: Theory and Practice. Elsevier/Academic Press, Burlington, (ISBN 978-0-12-078142-3).

[2] Srinivasan, S. (2006). Fuel cells: From Fundamentals to Applications. Springer Science-Business Media LLC.

[3] Sammes, N. (2006). Fuel Cell Technology. Springer Verlag, London.

[4] Lee, J. S., Quan, N. D., Hwang, J. M., Lee, S. D., Kim, H., Lee, H., Kim, H. S. (2005). Polymer electrolyte membranes for fuel cells. Journal of Industrial and Engineering Chemistry, 12(2), 175-183.

[5] Contestabile, M. (2010). Analysis of the market for diesel PEM fuel cell auxiliary power units onboard long-haul trucks and of its implications for the large-scale adoption of PEM FCs. Energy Policy, 38(10), 5320-5334.

[6] Lutsey, N., Brodrick C.-J., Lipman, T. (2007). Analysis of potential fuel consumption and emissions reductions from fuel cell auxiliary power units (APUs) in long-haul trucks. Energy, 32(12), 2428-2438.

[7] Brodrick, C. -J., Lipman, T. E., Farshchi, M., Lutsey, N. P., Dwyer, H. A., Sperling, D., Gouse, S. W., III, Harris, D. B., King, F. G. (2002). Evaluation of fuel cell auxiliary power units for heavy-duty diesel trucks. Transportation Research Part D: Transport and Environment, 7(4), 303-315.

[8] Barelli, L., Bidini, G., Ottaviano, A. (2012). Optimization of a PEMFC/battery pack power system for a bus application. Applied Energy, 97, 777-784.

[9] Bensaid, S, Specchia, S., Federici, F., Saracco, G., Specchia, V. (2009). MCFC-based marine APU: Comparison between conventional ATR and cracking coupled with SR integrated inside the stack pressurised vessel. International Journal of Hydrogen Energy, 34(4), 2026-2042.

[10] Kickulies, M. (2005). Fuel cell power for maritime applications, Fuel Cells Bulletin, 2005(9), 12-15.

[11] Beckhaus, P., Dokupil, M., Heinzel, A., Souzani, S., Spitta, C. (2005). On-board fuel cell power supply for sailing yachts. Journal of Power Sources, 145(2), 639-643.

[12] Vasallo, M. J., Bravo, J. M., Andújar, J. M. (2013). Optimal sizing for UPS systems based on batteries and/or fuel cell. Applied Energy, 105, 170-181.

[13] Silva, S. B., Severino, M. M., de Oliveira, M. A. G. (2013). A stand-alone hybrid photovoltaic, fuel cell and battery system: A case study of Tocantins, Brazil. Renewable Energy, 57, 384-389.

[14] Engelhardt, P., Maximini, M., Beckmann, F., Brenner, M. (2012). Integrated fuel cell APU based on a compact steam reformer for diesel and a PEMFC. International Journal of Hydrogen Energy, 37(18), 13470-13477.

[15] Pratt, J.,W., Klebanoff, L.,E., Munoz-Ramos, K., Akhil, A.,A., Curgus, D.,B., Schenkman, B.,L.. (2013). Proton exchange membrane fuel cells for electrical power generation on-board commercial airplanes, Applied Energy, vol 101, pp 776-796.

[16] Xu, X., Li, P., Shen, Y. (2013). Small-scale reforming of diesel and jet fuels to make hydrogen and syngas for fuel cells: A review, Applied Energy, Vol 108, pp 202-217.

[17] Ercolino, G., Ashraf, M.,A., Specchia, V., Specchia, S. (2015). Performance evaluation and comparison of fuel processors integrated with PEM fuel cell based on steam or autothermal reforming and on CO preferential oxidation or selective methanation, Applied Energy, Vol 143, pp 138-153.

[18] Agnolucci, P. (2007). Prospects of fuel cell auxiliary power units in the civil markets. International Journal of Hydrogen Energy, 32(17), 4306-4318.

[19] Severin, C., Pischinger, S., Ogrzewalla, J. (2005). Compact gasoline fuel processor for passenger vehicle APU. Journal of Power Sources, 145(2), 675-682.

[20] Aicher, T., Lenz, B., Gschnell, F., Groos, U., Federici, F., Caprile, L., Parodi, L. (2006). Fuel processors for fuel cell APU applications. Journal of Power Sources, 154(2), 503-508.

[21] FCGEN (Fuel Cell Based On-board Power Generation) (2011). FCH JU European project. Available at: http://www.fch-ju.eu/project/fuel-cell-based-board-power-generation

[22] DESTA project to demonstrate European SOFC truck APU (2012). Fuel Cells Bulletin, 5, p. 4.

[23] PURE (development of auxiliary Power Unit for Recreational yachts) FCH JU European project. Available at: http://www.fch.europa.eu/project/development-auxiliary-power-unit-recreational-yachts

[24] Jovan, V., Perne, M., Petrovčič, J. (2010). An assessment of the energetic flows in a commercial PEM fuel-cell system. Energy Conversion and Management, 51, 2467-2472.

[25] Ramos-Paja, C. A., Bordons, C., Romero, A., Giral, R., Martínez-Salamero, L. (2009). Minimum fuel consumption strategy for PEM fuel cells. IEEE Transactions on industrial electronics, 56(3), 685-696.

[26] Wikipedia – the free encyclopedia, https://en.wikipedia.org/wiki/Total_cost_of_ownership

[27] Mengel, C., Konrad, M., Wruck, R., Lucka, K., Köhne, H. (2008). Diesel steam reforming for PEM fuel cells. Journal of Fuel Cell Science and Technology, 5(2).

[28] Pregelj, B., Vrečko, D., Jovan, V. (2011). Improving the operation of a fuel-cell power unit with supervision control: A simulation study. Journal of Power Sources, 196(22), 9419-9428.

[29] Zhang, L., Jiang, J., Cheng, H., Deng, Z, Li, X. (2015). Control strategy for power management, efficiency-optimization and operating-safety of a 5-kW solid oxide fuel cell system. Electrochimica Acta, Volume 177, Pages 237-249.

[30] Gruber, J. K., Doll, M., Bordons, C. (2009). Design and experimental validation of a constrained MPC for the air feed of a fuel cell. Control Engineering Practice, 17(8), 874-885

[31] Krekel, D., Samsun, R.C., Pasel, J., Prawitz, M., Peters, R., Stolten, D. (2016). Operating strategies for fuel processing systems with a focus on water-gas shift reactor stability. Applied Energy, vol 164, 540-552.

[32] Debenjak, A., Petrovčič, J., Boškoski, P., Musizza, B., Juričić, Đ. (2015) Fuel cell condition monitoring system based on interconnected DC-DC converter and voltage monitor. IEEE transactions on industrial electronics, vol. 62, no. 8, pp 5293-5305.

[33] Boškoski, P., Debenjak, A. (2014). Optimal selection of proton exchange membrane fuel cell condition monitoring thresholds. Journal of Power Sources, 268, 692-699.

[34] Hu, X., Johannesson, L., Murgovski, N., Egardt, B. (2015). Longevity-conscious dimensioning and power management of the hybrid energy storage system in a fuel cell hybrid electric bus, Applied Energy, Vol 137, pp 13–924.

[35] Xu, L., Mueller, C.,D., Li, J., Ouyang, M., Hu, Z. (2015). Multi-objective component sizing based on optimal energy management strategy of fuel cell electric vehicles, Applied Energy, Vol 157, pp 664-674.

[36] Mulder G., Six, D., Claessens, B., Broes, T., Omar, N., Van Mierlo, J., (2013). The dimensioning of PV-battery systems depending on the incentive and selling price conditions Applied Energy, Vol 111, pp 1126-1135.

[37] Beck T., Kondziella, H., Huard, G., Bruckner, T. (2016). Assessing the influence of the temporal resolution of electrical load and PV generation profiles on self-consumption and sizing of PV-battery systems, Applied Energy, Vol 173, pp 331-342.

[38] Ogunjuyigbe, A.S.O., Ayodele, T.R., Akinola, O.A. (2016). Optimal allocation and sizing of PV/Wind/Split-diesel/Battery hybrid energy system for minimizing life cycle cost, carbon emission and dump energy of remote residential building, Applied Energy, Vol 171, pp 153-171.

[39] Pregelj B., Vrečko, D., Petrovčič, J., Dolanc, G., Jovan, V. (2015). A model-based approach to battery selection for truck onboard fuel cell-based APU in an anti-idling application. Applied Energy, 137, 64-76.

[40] Rahman, S. M. A., Masjuki, H. H., Kalam, M. A., Abedin, M. J., Sanjid, A., Sajjad, H. (2013). Impact of idling on fuel consumption and exhaust emissions and available idle-reduction technologies for diesel vehicles: A review. Energy Conversion and Management, 74, 171-182.

[41] Jain, S., Chen, H.-Y., Schwank, J. (2006). Techno-economic analysis of fuel cell auxiliary power units as alternative to idling. Journal of Power Sources, 160(1), 474-484.

[42] Pasel, J., Samsun, R. C., Peters, R., Stolten, D. (2013). Fuel processing of diesel fuel and kerosene for auxiliary power unit applications. Energy and Fuels, 27, 4386-4394.

[43] Pasel, J., Samsun, R.C., Tschauder, A., Peters, P., Stolten, D. (2015). A novel reactor type for autothermal reforming of diesel fuel and kerosene. Applied Energy, 150, 176-184.

[44] Samsun, R. C., Pasel, J., Janßen, H., Lehnert, W., Peters, R., Stolten, D. (2014). Design and test of a 5 kWe high-temperature polymer electrolyte fuel cell system operated with diesel and kerosene. Applied Energy, vol 114, 238-249.

[45] O'Connell, M., Kolb, G., Schelhaas, K.P., Schuerer, J., Tiemann, D., Ziogas, A., Hessel, V. (2010). The development and evaluation of microstructured reactors for the water gas shift and preferential oxidation reactions in the 5 kW range. International Journal of Hydrogen Energy, 35(6), 2317-2327.

[46] S2 Fuel Cell Data Sheet, Powercell AB (no date). Available at: http://www.powercell.se/wp-content/uploads/2015/09/S2_Fuel_Cell-150409.pdf

[47] Mathworks, MATLAB/Simulink/SimPowerSystems/Battery model, http://www.mathworks.com/help/physmod/sps/powersys/ref/battery.html.

[48] Pregelj, B., Mcguniness, D. T., Petrovčič, J., Dolanc, G., Jovan, V. (2015) Optimization of diesel powered FC-based APU size and battery capacity for specified load demand. *In proc of* 5th European PEFC & H2 Forum 2015, 30 June - 3 July 2015, Lucerne, Switzerland, pp 112-118.

[49] Qualion battery specification (no date). Available at: http://www.quallion.com/images-pdf/24V-%20QLD0100-MT.pdf

[50] Reinout Vader (2007). Energy Unlimited: The Book. Revision 9. Victron Energy B.V.

[51] Crompton, T. R. (2000). Battery Reference Book. 3rd ed. Reed Educational and Professional Publishing Ltd, Oxford.

[52] Dolanc, G., Pregelj B., Petrovčič, J., Pasel, J., Kolb, G. (2016). Control of autothermal reforming reactor of diesel fuel. Journal of Power Sources, 313, 223-232.

[53] Vrančič, D, Strmčnik, S, Juričić, D. (2001). A magnitude optimum multiple integration method for filtered PID controller. Automatica, 37, 1473-1479.